Structure

Article

Cobalamin decyanation by the membrane transporter BtuM

Graphical abstract

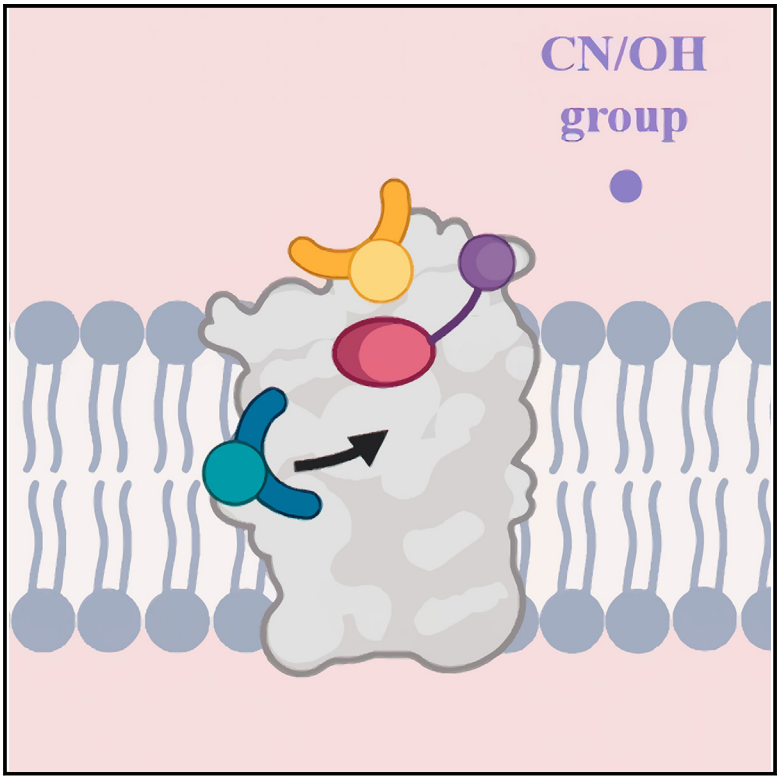

Authors

Jose M. Martínez Felices, Yan Borges Barreto, Chancievan Thangaratnarajah, Jacob J. Whittaker, Adriano M. Alencar, Albert Guskov, Dirk J. Slotboom

Correspondence

d.j.slotboom@rug.nl

In brief

Martínez Felices et al. reveal the structural basis of the covalent association between BtuM, a bacterial transporter, and its substrate cobalamin (vitamin B12). The binding kinetics, in which the substrate is chemically altered, was elucidated using spectrometric techniques and a mathematical modeling approach.

Highlights

- Cobalamin transporter BtuM structures reveal His28 as native β-axial coordinate
- Experiments and kinetic modeling reveal a two-step binding mechanism
- Weak and reversible initial substrate binding is followed by covalent trapping
- Substrate remains covalently bound after binding, obscuring the transport mechanism

Martínez Felices et al., 2024, Structure *32*, 1165–1173
August 8, 2024
https://doi.org/10.1016/j.str.2024.04.014

CellPress

Structure

CellPress

Article

Cobalamin decyanation by the membrane transporter BtuM

Jose M. Martínez Felices,[1] Yan Borges Barreto,[1,2] Chancievan Thangaratnarajah,[1] Jacob J. Whittaker,[1] Adriano M. Alencar,[2] Albert Guskov,[1] and Dirk J. Slotboom[1,3,*]

[1]Groningen Biomolecular and Biotechnology Institute (GBB), University of Groningen, Nijenborgh 4, Groningen 9474 AG, the Netherlands

[2]Instituto de Física, Universidade de São Paulo, São Paulo 05508-090, São Paulo, Brazil

[3]Lead contact

*Correspondence: d.j.slotboom@rug.nl

https://doi.org/10.1016/j.str.2024.04.014

SUMMARY

BtuM is a bacterial cobalamin transporter that binds the transported substrate in the base-off state, with a cysteine residue providing the α-axial coordination of the central cobalt ion via a sulfur-cobalt bond. Binding leads to decyanation of cobalamin variants with a cyano group as the β-axial ligand. Here, we report the crystal structures of untagged BtuM bound to two variants of cobalamin, hydroxycobalamin and cyanocobalamin, and unveil the native residue responsible for the β-axial coordination, His28. This coordination had previously been obscured by non-native histidines of His-tagged BtuM. A model in which BtuM initially binds cobinamide reversibly with low affinity (K_D = 4.0 μM), followed by the formation of a covalent bond (rate constant of 0.163 s^{-1}), fits the kinetics data of substrate binding and decyanation of the cobalamin precursor cobinamide by BtuM. The covalent binding mode suggests a mechanism not used by any other transport protein.

INTRODUCTION

Genomic analyses have shown that more than three-quarters of bacterial species harbor cobalamin-dependent enzymes to catalyze a variety of metabolic reactions.[1,2] Despite this widespread use as a cofactor, *de novo* biosynthesis of cobalamin is restricted to a limited number of bacterial and archaeal species.[3] Consequently, organisms that rely on cobalamin-dependent enzymes, but lack the capacity to synthesize the cofactors themselves, have to acquire cobalamin from external sources, a process that requires membrane transporters.[4]

Only a single protein (BtuB) is known to transport cobalamin across the outer membrane of gram-negative bacteria,[5] but the repertoire of membrane transport systems for cobalamin in the plasma membrane of gram-negative and -positive bacteria is more extensive. Three different families of proteins belonging to the superfamily of adenosine tri-phosphate (ATP)-binding cassette (ABC) transporters have been shown to transport cobalamin: BtuCDF (a type II ABC transporter),[6] ECF-CbrT (type III),[7,8] and Rv1819c (type IV).[4,9,10] The recently discovered protein BtuM is the only known protein involved in cobalamin transport that does not belong to the ABC transporter superfamily.[11] Nonetheless, a crystal structure of BtuM surprisingly revealed that the protein is structurally related to the substrate-binding units (S-components) found in type III or energy-coupling factor (ECF)-type ABC transporters, a family that also includes the aforementioned ECF-CbrT. In ECF transporters, the S-component forms a complex with a so-called ECF module consisting of an ATPase dimer and membrane inserted subunit T. Surprisingly, organisms that contain BtuM lack the genes encoding the ECF module.[11] BtuM has thus been classified as a "solitary" S-component based on its structural homology, which is a subgroup of ECF-type ABC transporters that can autonomously transport substrates across the membrane without the need of an ECF module and ATP hydrolysis.[11,12] However, the transport mechanism remains largely unknown.

In aqueous solution, the α-axial ligand of the central cobalt atom in free cobalamin is the 5,6-dimethylbenzimidazole (DMB) group, which is covalently attached to the corrin ring.[13,14] At physiological pH, this so-called base-on conformation is strongly favored over the base-off conformation in which the DMB group is detached from the central cobalt ion.[15] In contrast, when bound to enzymes using cobalamin as cofactor, the DMB ligand is usually replaced by a group from the protein, and cobalamin is kept in the base-off conformation. At the opposite face of the corrin ring, the β-axial position of free cobalamin may be a hydroxyl group (hydroxycobalamin, OHCbl) or cyano group (cyanocobalamin, CNCbl). The biological relevance of the cyano group in CNCbl is unknown, but it is the cofactor form commonly used in multivitamin formulations. The cobalamin precursor cobinamide (Cbi) lacks the DMB moiety coordinating the central cobalt ion and can accommodate cyano

groups at both axial positions. Decyanation of CNCbl is a prerequisite for its conversion to the active cofactor forms in enzymes, in which the cyano ligand is replaced by a methyl group (in methylcobalamin) or a 5′-deoxyadenosyl group (in coenzyme B_{12} or 5′-deoxyadenosylcobalamin).[13]

The crystal structure of BtuM revealed a bound cobalamin molecule in a base-off conformation,[11] a binding mode typically observed in proteins with enzymatic activity[16,17] but not previously observed in cobalamin transporters. In complex with BtuM, the DMB base is replaced by a cysteine residue that forms a rare sulfur-cobalt bond. A sulfur-cobalt bond has also been reported in the cobalamin chaperone and trafficking complex CblC-CblD,[18] but in this case, the cysteine is the β-axial ligand[19] and in complexes of cobalamin with monoclonal antibodies,[20] in which case the binding mode is unknown. The interaction between BtuM and CNCbl results in the removal of the cyano group from the β-axial position,[11] a process in which cysteine ligation of the cobalt ion is essential. Protein-mediated modification of the precursor Cbi by BtuM has also been confirmed.[11] The transport mechanism of BtuM and the mechanistic importance of decyanation for transport are not yet understood.

The previously solved structure of BtuM contained a crystallization artifact, with the C-terminal His-tag of BtuM found in the ligand binding site of a neighboring BtuM molecule in the crystal. One of the histidines from the His-tag coordinates the cobalt ion at the β-axial position. In this work, we solved the crystal structures of untagged BtuM bound to two of its substrates, OHCbl and CNCbl, revealing the native β-axial ligand, His28. We also provide spectroscopic and kinetic information on the binding mechanism of the two cobalamin variants, CNCbl and OHCbl, as well as the precursor Cbi. The kinetic analysis is consistent with a two-step binding mechanism, where BtuM initially binds Cbi reversibly (K_D = 4.0 μM), to then form a covalent bond (rate constant of 0.163 s^{-1}). The conversion of the DMB moiety from the base-on to base-off conformation constitutes a potential kinetic bottleneck and makes the binding of the cobalamin precursor Cbi faster compared to cobalamin variants CNCbl and OHCbl.

RESULTS

Histidine 28 coordinates cobalamin in the β-axial position

We engineered a BtuM variant that incorporates a cleavage site (LEVLFQ/GP), recognized by the human rhinovirus protease 3C (abbreviated 3C), between the N-terminal His-tag, which had previously caused the undesired artifact[11] and the BtuM protein. Upon purification and cleavage with protease 3C, we obtained the BtuM protein with only two additional residues (GP) at the N terminus, eliminating any possible artifacts caused by the His-tag (Figure S1A).

We used X-ray crystallography to solve the structures of detergent-solubilized BtuM bound to either CNCbl or OHCbl at 3.0 and 2.26 Å resolution, respectively (Table 1). The overall fold of BtuM in both structures is identical (root-mean-square deviation [RMSD] 0.22 Å). Structural alignment with the previously solved structure of His-tagged BtuM[11] also reveals overall similar folds with RMSD values of 0.61 and 0.68 Å, respectively (Figure 1A). In both new structures, the DMB moiety, which is the α-axial ligand of free cobalamin, adopts the base-off conformation (Figure S2), exposing its α-coordination site for an interaction with cysteine residue 80 (Figure 1C).[4] The distance between the sulfur atom of Cys80 and the cobalt ion is 2.4 Å, similar to what was observed in the structure of the His-tagged protein.[11] Although sulfur-cobalt bonds are labile,[19] the adduct has been detected by mass spectrometry.[11] In the structure of untagged BtuM, the β-axial ligands of cobalamin (hydroxy and cyano groups of OHCbl and CNCbl, respectively) have been replaced by a native BtuM residue, histidine 28, which coordinates the cobalt ion using the ε nitrogen atom (Nε). Because the hydroxy and cyano groups were removed from cobalamin upon binding to BtuM, the bound compounds in the two structures are identical, and we will base the rest of our interpretation on the structure determined to the highest resolution (OHCbl, solved at 2.26 Å resolution). The distance between the Nε of His28 and the central cobalt ion is 2.1 Å, shorter than other nitrogen-cobalt distances observed in previously reported cobalamin structures in the base-off conformation, ranging from 2.3 to 2.6 Å.[21–23] The bond between Nε of His28 and the cobalt ion of cobalamin on the β-axial side is at 165° angle with the sulfur-cobalt bond on the α-axial side (Figure 1C). A role for His28 as a cobalamin-coordinating residue was previously hypothesized by Rempel et al.[11]

The most prominent differences between the new untagged structures and the previously determined structure of His-tagged BtuM involve the transmembrane helix 1 (TM1) and loop 1 connecting TM1 and TM2, which contains His28. In the untagged structures, the N-terminal end of TM1-loop is tilted away from the protein core by approximately 20°, while loop 1 has moved toward the bound substrate (Figure 1B). In this way, the coordinating residue His28 is positioned at the β surface of Cbl (Figures 1B and 1C). Loop 1 in the previously solved structure of His-tagged BtuM contained α-helical secondary structure around His28, and the histidine was located 14.3 Å away from the cobalt ion. Therefore, the structural analysis may suggest that the interaction of BtuM with Cbl disrupts the secondary structure in loop 1, allowing for the closer approach of the β-axial ligand of Cbl (Figures 1A and 1B), or that the binding of His28 to the β-axial position disrupts the secondary structure. It can also not be excluded that the previously observed α-helical secondary structure around His28 was an artifact of the His-tag in the BtuM construct used.

Mutants for histidine 28 maintain their ability to transport CNCbl

To investigate the functional significance of the coordination by His28, we mutated the residue into alanine and assessed the ability of the mutant variant to transport Cbl into cells. Additionally, the neighboring histidine 27 was also mutated to alanine in a H27A/H28A double-mutant variant, as we reasoned that the flexibility of loop 1 might allow recruitment of His27 as β-axial ligand in the absence of the native His28 side chain. Per note, His28 is highly conserved, whereas His27 is not that well conserved.[11]

To evaluate the transport efficiency of these mutant variants *in vivo*, growth assays were performed using *E. coli* ΔFEC strains, which lack the endogenous cobalamin transporter BtuCDF and the cobalamin-independent methionine synthase MetE. This strain requires methionine in the culture medium to

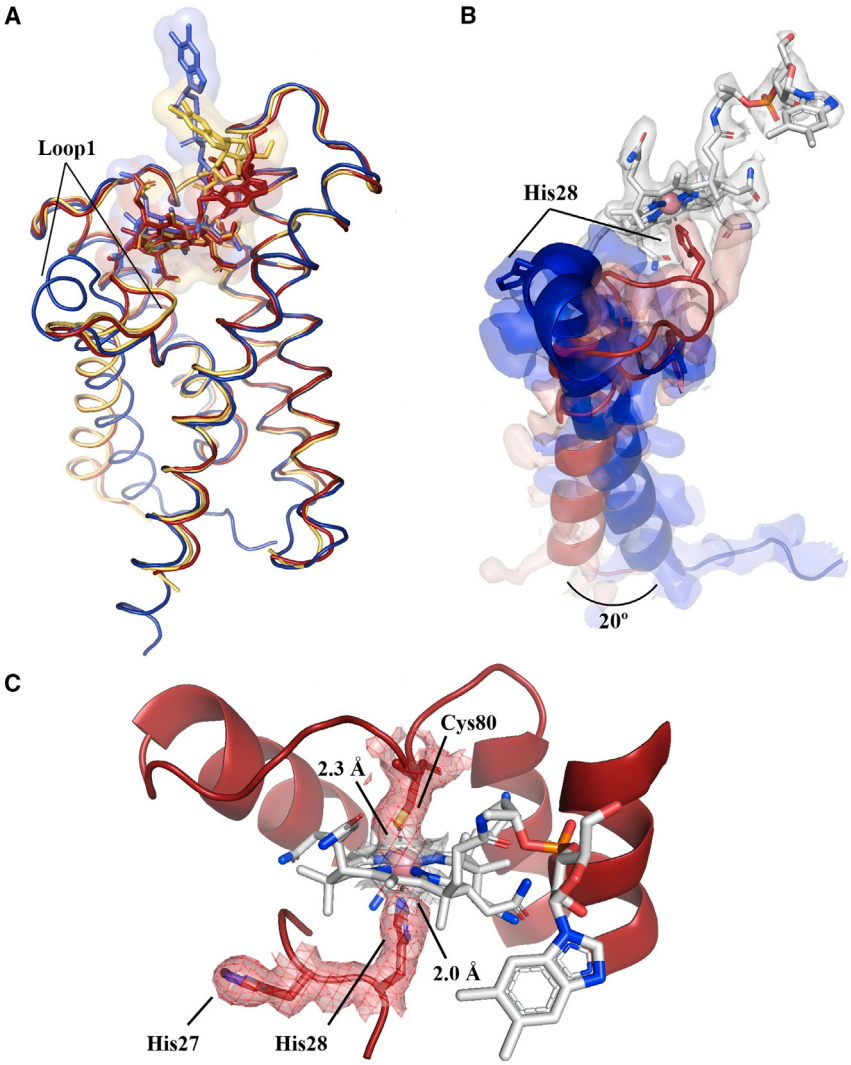

Figure 1. Crystal structures of OHCbl-BtuM and CNCbl-BtuM

(A) Backbone alignment between a previously solved His-tagged BtuM structure (blue, PDB: 6ffv), and the in-here reported untagged BtuM structures (purified in presence of OHCbl, [red] or CNCbl-BtuM [yellow]). The protein is shown in ribbon representation and the cobalamin ligand in stick representation with volumes for electron densities at a σ level of 3.0.

(B) Zoom-in onto the transmembrane helix 1 and loop 1 in the secondary structure cartoon representation with 6ffv in blue and tagless BtuM purified in the presence of OHCbl in red.

(C) Cartoon representation of the binding site of OHCbl-BtuM. The side chains of Cys80, His27, and His28 are shown as sticks and axial coordination distances labeled. Volumes with mesh represent the electron densities at a σ level of 3.0.

grow. In the absence of methionine, the strain can survive only if it can take up cobalamin so that methionine can be synthesized by the cobalamin-dependent methionine synthase MetH.[11] The strain was transformed with expression plasmids for wild-type or mutant BtuM and cultivated in a minimal medium containing 0.1 nM CNCbl (Figure 2A). As a negative control, the inactive mutant of BtuM C80S, in which the α-axial cysteine is replaced by serine, was used. Cells producing wild-type BtuM, the single-mutant variant H28A or the double-mutant variant H27A/H28A, all showed similar growth rates and reached similar cell densities, indicating efficient transport of cobalamin (Figure 2A), while the C80S mutant variant showed very poor growth. Thus, these results indicate that a coordinating histidine is not essential for transport and growth *in vivo*, whereas Cys80 is.

Furthermore, decyanation assays (described in the following section) were performed *in vitro* on the histidine mutant variants H27A/H28A, which showed similar results as the wild type, indicating that the coordinating histidine residues are not required for the removal of the cyano group from CNCbl (Figures S3A and S3B). Taken together, these findings suggest that despite His28 coordinates for cobalamin in the wild-type BtuM, it is actually not strictly required for cobalamin transport and utilization by the cell.

The "unlocking" of the DMB moiety of cobalamin is the kinetic bottleneck during binding

In all solved BtuM structures (Figure 1), the Nε from a histidine residue is the β-axial ligand of the bound cobalamin, which means that the original β-axial ligands present in the free substrates OHCbl and CNCbl (OH- and CN-, respectively) had been removed upon binding. Decyanation or dehydroxylation is caused by reduction of the cobalt ion upon coordination by the sulfur from Cys80.[11] Here, we used two spectroscopic techniques to provide insight into this binding event from two perspectives: we recorded absorbance spectra of cobalamin or Cbi, where spectral changes are indicative of decyanation, and we recorded intrinsic protein (tryptophan) fluorescence spectra, where quenching reports on changes in the protein environment upon substrate binding.

For the cobalamin precursor Cbi, the decyanation activity of BtuM has been demonstrated using the absorbance-based assay *in vitro* by following the decrease of the peak at 367 nm (Figure 2D).[11] Decyanation or dehydroxylation have not been demonstrated for the complete cobalamin molecule (CNCbl or OHCbl), but these reactions can be monitored as a decrease of the absorption at the maxima at 351 and 361 nm for OHCbl and CNCbl, respectively (Figures 2B and 2C). We monitored the spectral changes over time upon addition of an excess of purified untagged BtuM to each substrate (Figures 2B–2D). Normalizing for values at the start of the experiment (no binding) and in saturating conditions (all substrate is bound), we derived the substrate saturation as the fraction of substrate (CNCbl, OHCbl, or Cbi) bound to BtuM (See STAR Methods). The rate of substrate saturation was different for Cbi and cobalamin variants (Figure 3A). The decyanation of Cbi by BtuM ($t_{1/2}$ = 14.5 ± 2.5 min) is faster than the

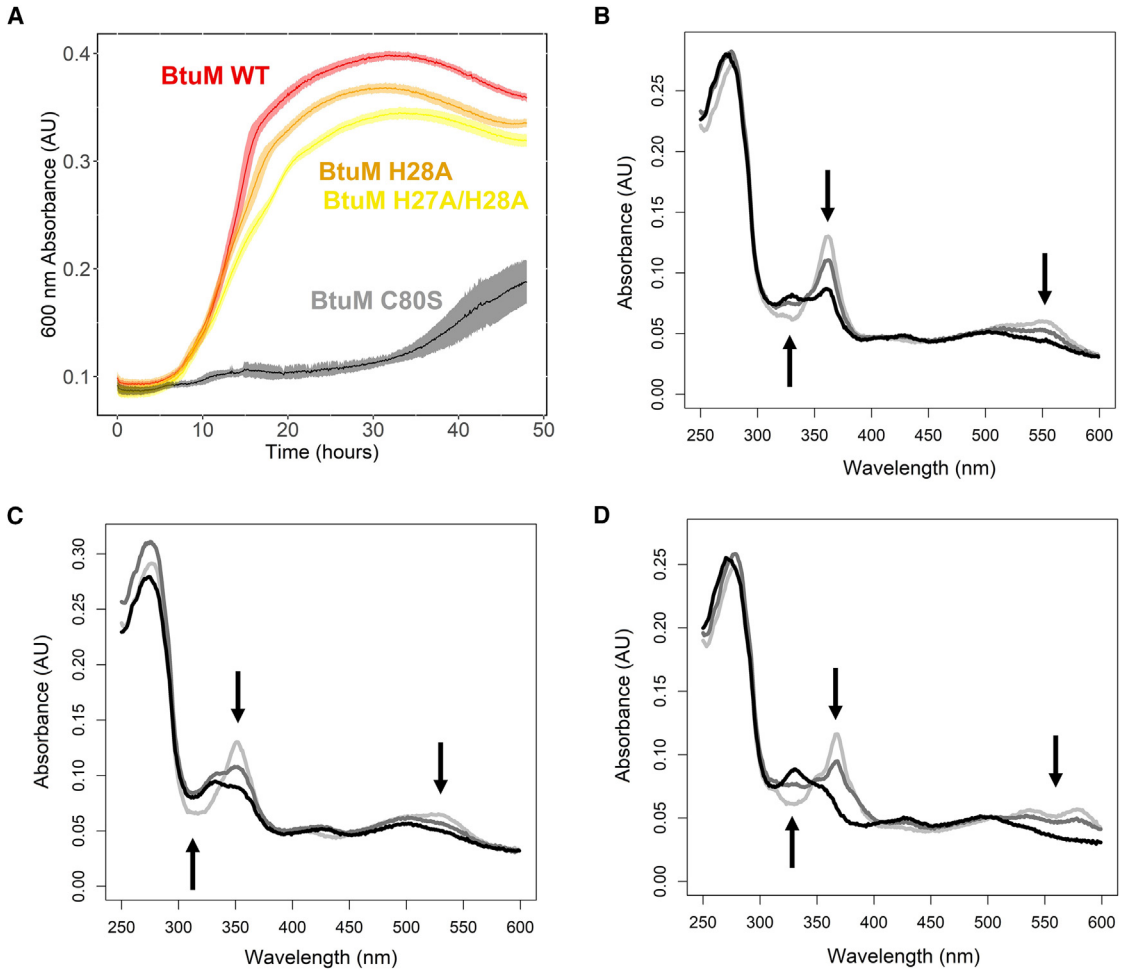

Figure 2. *In vivo* complementation of BtuM in ΔFEC *E. coli* strains and spectral changes in cobalamin variants upon BtuM binding

(A) Growth curves for *E. coli* ΔFEC strains transformed with wild-type BtuM (red), BtuM C80S (gray), BtuM H28A (orange), and BtuM H27A/H28A (yellow) grown in enriched M9 minimum medium (see STAR Methods) supplemented with 0.1 nM CNCbl. Curves are averages of technical triplicates of biological duplicates. Shadows are standard deviation errors for each curve.

(B) Absorbance scans for CNCbl, OHCbl (C), and Cbi (D) upon addition of BtuM at a 3:1 protein:substrate ratio in detergent solution. Lines in gray represent initial and intermediate states and in black the final state of a >10-h incubation.

modification of OHCbl ($t_{1/2}$ = 56.0 ± 20.7 min) and CNCbl ($t_{1/2}$ = 58.0 ± 21.7 min).

To gain further insight into the kinetics underlying BtuM:substrate interaction and the decyanation/dehydroxylation process, we also performed tryptophan fluorescence measurements.[24,25] BtuM contains a total of five tryptophan residues, the fluorescence of two of which (Trp29 and Trp40) is expected to be sensitive to substrate binding because they directly face the binding site (Figure S4A). Tryptophan fluorescence of BtuM decreased upon incubation with cobalamin and Cbi substrates (Figure S4B). Similar to what was observed in the absorbance-based assay (see the text described previously, Figures 2A–2C), the rate of fluorescence quenching was also different for the three substrates tested. The rate of BtuM binding to Cbi, as measured in the fluorescence assays, was similar to the rate of absorbance decay ($t_{1/2}$ = 10.3 ± 1.3 min) (Figures 3A and 3B). The binding rates to OHCbl and CNCbl could not be calculated from the fluorescence measurement due to long saturation times (>12 h), disturbing the signal, probably due to bleaching of the protein.

The differences in rates of modification of cobalamin and Cbi may be explained by the absence of DMB moiety in the latter compound (Figure S2). BtuM binds cobalamin in the base-off form (Figure 1C). Therefore, the DMB moiety needs to be displaced by Cys80 to coordinate the central cobalt ion of cobalamin. This step may be rate limiting. In the case of Cbi, the DMB is absent, hence Cys80 binding to the central cobalt ion is faster.

In vitro cobalamin binding to BtuM is irreversible

To further investigate the substrate modification process mediated by BtuM, we analyzed the kinetics of binding and decyanation at different protein and substrate concentrations (Figures 3C, 3D, S3C, and S3D). The substrate saturation in the absorbance assay increases with the concentration of incubated

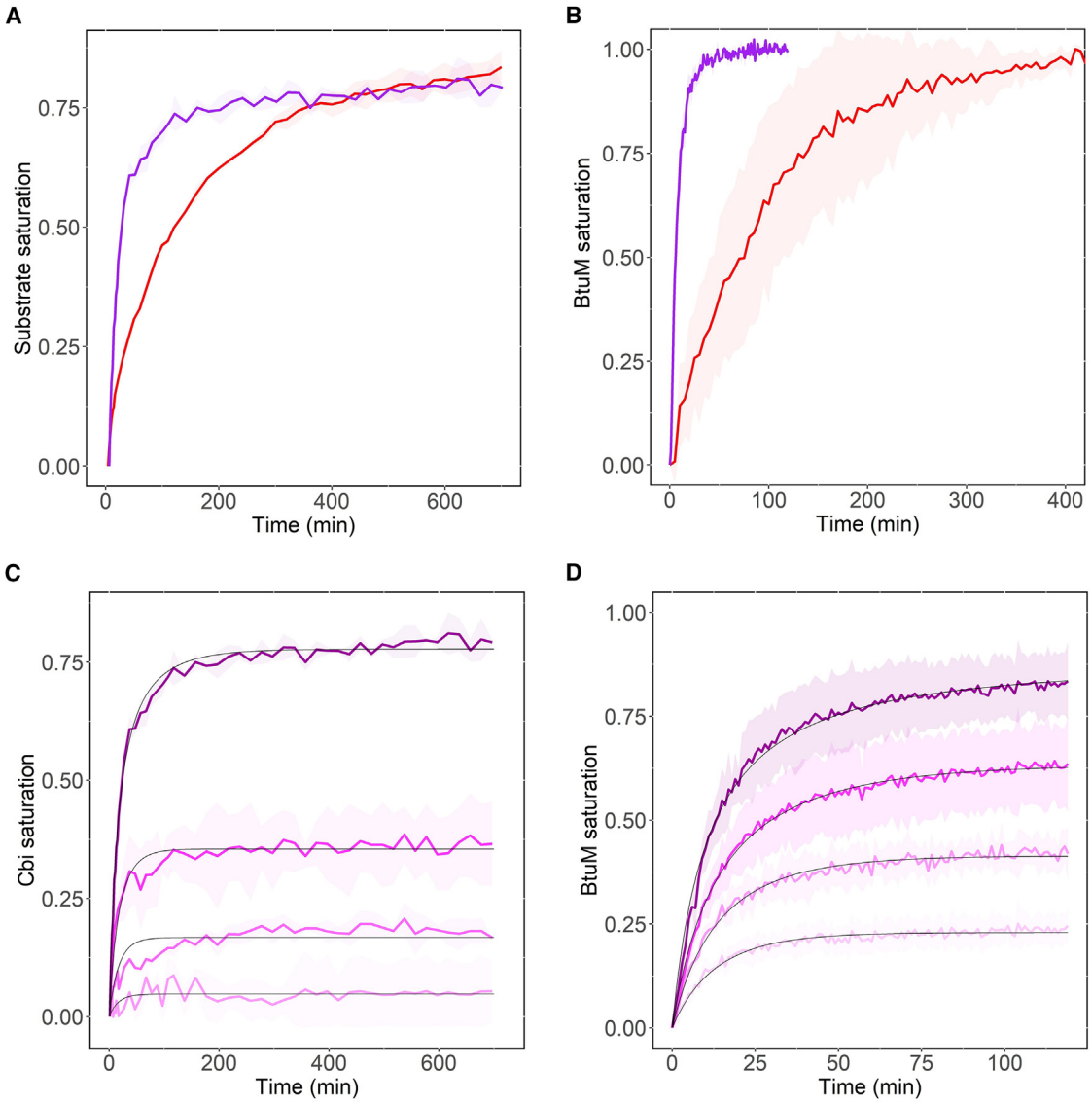

Figure 3. Kinetic analysis of the BtuM-B_{12} interaction

Absorbance-detected substrate saturation of (A) 5 μM Cbi (purple) and 5 μM OHCbl (red) incubated with 4 μM BtuM; and (C) 5 μM Cbi incubated with 0.5, 1, 2, and 4 (as in A) μM BtuM (lighter to darker purple lines, respectively).

(B) Fluorescence-detected BtuM saturation of 100 nM BtuM incubated with (B) 200 nM Cbi (purple) and 200 nM OHCbl (red) and (D) 20, 40, 60, and 80 nM Cbi (lighter to darker purple lines, respectively). All panels show normalized data with a value of one representing the maximally observed level of change in fluorescence or absorbance. Non-normalized absorbance and fluorescence spectra can be found in Figures 2 and S4, respectively. Absorbance curves are averages of two technical replicates. Fluorescence curves are averages of four independent replicates. Ribbon represents one standard deviation. Black lines represent the fitted two-step irreversible binding model.

BtuM (Figure 3C). Consistently, the BtuM saturation increases with the concentration of incubated Cbi (Figure 3D).

To model the results of absorbance and fluorescence assays, we developed a *de novo* kinetic model that could fit our data to a 1:1 two-step irreversible binding interaction (Suppl. Info., Equation 13). This mechanism has two main components: a reversible interaction characterized by the dissociation constant K_D, followed by an irreversible binding, which is characteristic for irreversible inhibitors and its rate constant is k_{23}[26] (Suppl. Info. 1). This model accounts for the depletion of protein and substrate that occurs when an irreversible binding event occurs in a closed environment like a quartz cuvette, with continuously decreasing concentrations of apo-protein and free substrate. The kinetic model yielded the kinetic constants K_D = 4.0 ± 0.2 μM for the reversible interaction between BtuM and Cbi and k_{23} = 0.163 ± 0.008 s^{-1} for the covalent interaction (for fits see Figures 3C and 3D, Suppl. Info. 1). The same experiment using cobalamin variants OHCbl and CNCbl could not be fitted so accurately to the data (Figure S3) mainly due to the long times to reach saturation, in the range from 10 to 16 h of incubation. Therefore, crystallographic and spectroscopic data further support the idea that unlocking the DMB moiety to coordinate the central cobalt

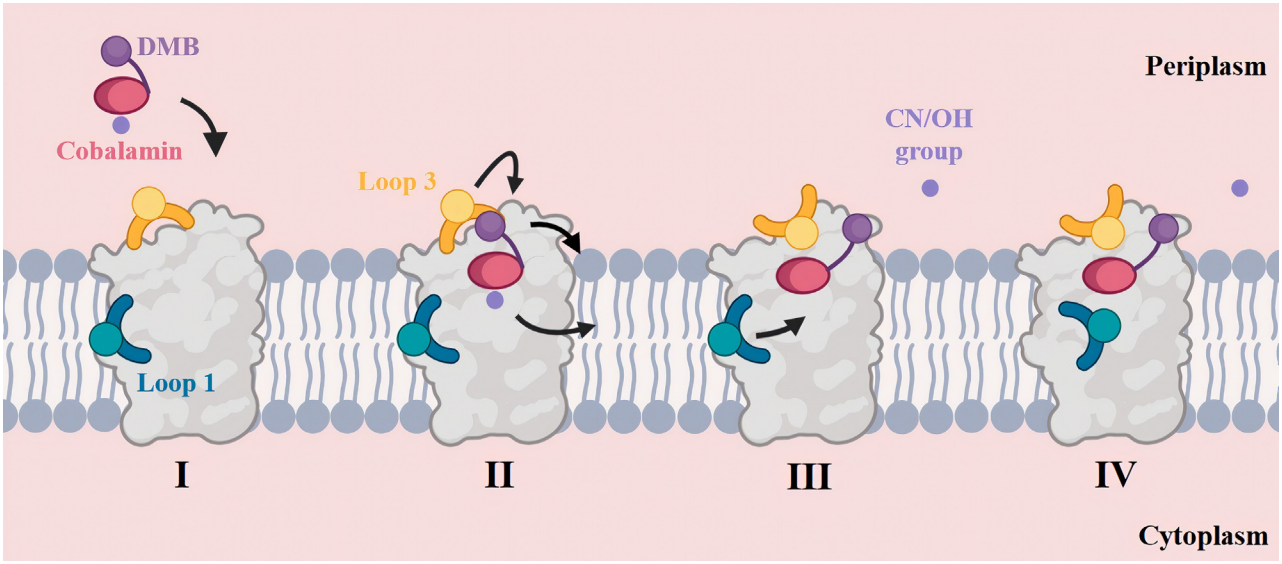

Figure 4. Model for cobalamin binding to BtuM

Schematic model of the interaction between BtuM and a cobalamin substrate. BtuM shown in gray embedded in a lipidic membrane, loop 1 in blue with histidine 28 as a ball, loop 3 in yellow with cysteine 80 as a ball, the corrin ring of cobalamin in red, attached to a purple ball at the α-side of the corrin ring as the DMB moiety, and a smaller lilac circle for the functional group at the β-side. Arrows represent molecular motions that lead to the next state.

ion is a critical kinetic barrier for irreversibly binding cobalamin variants.

DISCUSSION

In this study, we report data supporting CNCbl and Cbi decyanation, OHCbl dehydroxylation by a wild-type, untagged version of BtuM *in vitro* based on crystallographic data, and absorbance and fluorescence spectroscopy (Figure 2). Crystal structures of BtuM in complex with two cobalamin variants, OHCbl and CNCbl (Figure 1A), confirm that Cys80 is the α-axial ligand of the central cobalt ion (Figure 1C), with which it forms a covalent bond. Reported structures also uncover the role of His28 as the native β-axial ligand of the central cobalt ion (Figure 1). Although being a highly conserved histidine, mutational studies showed that this His28 is neither essential for transport *in vivo* (Figure 2A), nor for decyanation *in vitro* (Figures S3A and S3B).

Covalent interactions between cobalamin and cysteine residues have been reported previously.[18,20] In addition, cobalamin inhibits Tau fibrillation via cysteine interaction, becoming a potential treatment against Alzheimer disease and neurodegeneration.[27] However, the binding mechanisms in these cases are either different, with a β-axial sulfur-cobalt bond in case of CblC-CblD,[19] or unresolved. BtuM displays slow binding kinetics for the cobalamin and Cbi substrates (Figure 3), which can be described by a two-step irreversible binding model (Suppl. Info 1). The BtuM:substrate complex formation was followed through both the fluorescence signal of BtuM and the absorbance of the substrate (Figure 3). In the conditions measured, BtuM can bind Cbi reversibly with a K_D of 4.0 ± 0.2 μM, similar to a previous dissociation constant reported for BtuM C80S inactive mutant of K_D = 5.6 ± 2.8 μM determined using isothermal titration calorimetry (ITC).[11] It is noteworthy that this value deviates from the apparent K_D value of 0.65 ± 0.27 μM for binding of Cbi to BtuM containing the native Cys at position 80, also determined by ITC.[11] The difference is likely caused by the subsequent covalent bond formation that prevents the initial binding reaction from reaching equilibrium. The rate constant for the subsequent irreversible step k_{23} is 0.163 ± 0.008 s^{-1}, considerably slower than irreversible constants measured on acylating inhibitors binding serine residues (2.6 s^{-1}).[28] Cysteines can be classified based on their reactivity,[29] where "hyperreactive" cysteines show rate constants for the irreversible reaction of 4.2 s^{-1} or higher, >20-fold higher than measured for the reaction between Cys80 and the precursor Cbi.[30] Surprisingly, cobalamin binding is much slower than that of Cbi (Figures 3A–3C). We hypothesize that the presence of a DMB moiety in cobalamin variants prevents the access of the Cys80 residue of BtuM to the central cobalt ion, while access to the ion in Cbi is unrestricted due to the lack of DMB.

Our findings allow us to propose a binding model with a covalent bond formation between the substrate and BtuM (Figure 4). Free aqueous cobalamin encounters *apo*-BtuM in the bacterial inner membrane (Figure 4, State I) and initially binds weakly via noncovalent interactions in a reversible way, with free- and B_{12}-bound BtuM in near equilibrium. Free cobalamin is mostly in the base-on state,[15] but binding eventually leads to "unlocking" of the DMB moiety of cobalamin variants. It is not clear if the initial binding to BtuM induces the unlocking or if the protein selects for the small fraction of free cobalamin in the "base-off" conformation. Either way, the unlocking of the DMB moiety likely represents the greatest kinetic bottleneck of cobalamin binding by BtuM.[31] Consistently, binding of the precursor Cbi, which lacks the DMB part, is faster than cobalamin binding (Figures 3A and 3B).

The initial contacts allow for the coordinating residues His28 and Cys80 to approach the substrate's central cobalt ion (Figure 4, state II). The coordination of Cys80 to the central cobalt

Table 1. Data collection and phasing and refinement statistics

	OHCbl-bound BtuM (PDB: 8OVV)	CNCbl-bound BtuM (PDB: 8C7P)
Wavelength (Å)	0.984	0.976
Resolution range (Å)	39.54–2.26 (2.33–2.26)	79.08–3.0 (3.18–3.0)
Space group	P 3_221	P 3_221
Unit cell (Å)	91.32, 91.32, 77.39	95.98, 95.98, 77.29
α, β, γ (°)	90, 90, 120	90, 90, 120
Total reflections	29,975 (1,130)	11,593 (622)
Unique reflections	15,828 (591)	6,264 (336)
Completeness (%)	80.4 (32.6)	80.69 (26.6)
Mean I/sigma (I)	15.8 (4.3)	11.2 (2.3)
Wilson B-factor	26.13	55.35
R-meas	0.092 (0.376)	0.131 (0.568)
R-pim	0.065 (0.266)	0.093 (0.402)
CC1/2	0.991 (0.731)	0.983 (0.747)
Reflections used in refinement	15,828 (591)	6,264 (336)
Reflections used for R-free	782 (31)	295 (15)
R-work	0.1816	0.225
R-free	0.2020	0.263
Number of non-hydrogen atoms	1,585	1,474
macromolecules	1,353	1,383
ligands	196	91
solvent	36	0
Protein residues	175	179
RMS (bonds) (Å)	0.0176	0.0123
RMS (angles) (°)	2.410	2.019
Ramachandran favored (%)	97.08	90.96
Ramachandran allowed (%)	2.92	9.04
Ramachandran outliers (%)	0.0	0.0
Rotamer outliers (%)	0.75	5.07
Clashscore	6.29	10.00
Average B-factor	36.69	81.0
macromolecules	35.86	81.36
ligands	41.63	84.66
solvent	43.38	0.00

ion releases the functional group on the opposite β-side that becomes available for coordination by His28 (Figure 4, State III). Once the β-axial functional group is removed, this ligand is replaced by the residue His28 (state IV). Whether this replacement takes place simultaneously with the removal of the original β-axial group or consecutively is not clear. Based on comparison of the structures of untagged and His-tagged BtuM, the native coordination at the β-axial position by His28 may lead to the disruption of the secondary structure in loop 1 in BtuM. This loop shifts from being away from the substrate forming an α-helix (Figure 1B, PDB: 6FFV), to coordinating the cobalt ion in a loop without secondary structure (Figure 1B, OHCbl-BtuM, Figure S4B). Similar loop 1 motions have also been reported for other structurally related ECF S-components like FolT[32] and ThiT,[33] where loop 1 acted as a "gate" at the binding site. In these S-components, loop 1 closure leads to occlusion of the transported substrates (folate for FolT and thiamine for ThiT). In contrast, closure of loop 1 in BtuM does not lead to cobalamin occlusion, and the substrate remains exposed to the aqueous environment on the periplasmic side of the membrane (Figure S5). Mutational analysis showed that coordination of cobalamin by histidines in loop 1 of BtuM is not essential for binding or transport (Figures 2A, S3A, and S3B). Possibly, water can take over the coordination of the reduced cob(II)alamin in the mutants.[34]

The physiological implications of the covalent interaction still remain unclear. In gram-negative organisms, the outer-membrane transporter BtuB is in charge of scavenging B_{12} from the environment and actively transporting it to the periplasm.[5] Integral membrane transporters in the cytoplasmic membrane then deliver the vitamin to the cytosol. The results of this work suggest a different role for BtuM compared to other inner membrane cobalamin transporters, namely BtuCDF and ECF-CbrT.[4] These act as scavengers by binding the substrate on the periplasmic side of the membrane with high affinity (low nanomolar K_D), yet non-covalently, and use the free energy from ATP binding and

hydrolysis to release the transported substrate in the cytoplasm. BtuM, however, binds the substrate covalently on the periplasmic side of the membrane with slow kinetics. One possibility is that the release of cobalamin from BtuM is assisted by a non-dedicated process like protein turnover and degradation, similar to what is needed for release of cobalamin from human intrinsic factor.[35] Furthermore, the reaction of cobalamin with BtuM, renders the substrate to be in its active cob(II)alamin form, which can be used as a metabolic cofactor. Nevertheless, future studies are necessary to understand this unique transport mechanism coupled to the chemical modification of a substrate. Moreover, such a coupled modification-transport mechanism might be exploited as a delivery system to allow cobalamin adducts to reach the cytoplasm.

STAR★METHODS

Detailed methods are provided in the online version of this paper and include the following:

- KEY RESOURCES TABLE
- RESOURCE AVAILABILITY
  - Lead contact
  - Materials availability
  - Data and code availability
- EXPERIMENTAL MODEL AND STUDY PARTICIPANT DETAILS
- METHOD DETAILS
  - Molecular methods
  - Overexpression and bacterial membranes preparation
  - Purification of BtuM
  - Crystallography experiments
  - Crystallisation, phasing and structure determination
  - Growth assay
  - Absorbance kinetic assay
  - Tryptophan fluorescence kinetic assay
- QUANTIFICATION AND STATISTICAL ANALYSIS

SUPPLEMENTAL INFORMATION

Supplemental information can be found online at https://doi.org/10.1016/j.str.2024.04.014.

AUTHOR CONTRIBUTIONS

Conceptualization, J.M.M.F. and D.J.S.; software, Y.B.B. and J.M.M.F.; formal analysis, J.M.M.F. and Y.B.B.; investigation, J.M.M.F. and J.J.W.; writing – original draft, J.M.M.F.; writing – review and editing, J.M.M.F., D.J.S., and A.G.; visualization, J.M.M.F. and C.T.; supervision, A.M.A., A.G. and D.J.S.

DECLARATION OF INTERESTS

The authors declare no competing interests.

Received: June 20, 2023
Revised: March 4, 2024
Accepted: April 15, 2024
Published: May 10, 2024

REFERENCES

1. Shelton, A.N., Seth, E.C., Mok, K.C., Han, A.W., Jackson, S.N., Haft, D.R., and Taga, M.E. (2019). Uneven distribution of cobamide biosynthesis and dependence in bacteria predicted by comparative genomics. ISME J. *13*, 789–804. https://doi.org/10.1038/s41396-018-0304-9.
2. Zhang, Y., Rodionov, D.A., Gelfand, M.S., and Gladyshev, V.N. (2009). Comparative genomic analyses of nickel, cobalt and vitamin B12 utilization. BMC Genom. *10*, 78. https://doi.org/10.1186/1471-2164-10-78.
3. Fang, H., Kang, J., and Zhang, D. (2017). Microbial production of vitamin B12: A review and future perspectives. Microb. Cell Factories *16*, 15. https://doi.org/10.1186/s12934-017-0631-y.
4. Nijland, M., Martínez Felices, J.M., Slotboom, D.J., and Thangaratnarajah, C. (2022). Membrane transport of cobalamin. In Vitamins and Hormones (Academic Press), pp. 121–148. https://doi.org/10.1016/BS.VH.2022.01.008.
5. Kadner, R.J., and Liggins, G.L. (1973). Transport of vitamin B12 in Escherichia coli: genetic studies. J. Bacteriol. *115*, 514–521. https://doi.org/10.1128/JB.115.2.514-521.1973.
6. DeVeaux, L.C., and Kadner, R.J. (1985). Transport of vitamin B12 in Escherichia coli: Cloning of the btuCD region. J. Bacteriol. *162*, 888–896. https://doi.org/10.1128/jb.162.3.888-896.1985.
7. Santos, J.A., Rempel, S., Mous, S.T., Pereira, C.T., Ter Beek, J., de Gier, J.-W.W., Guskov, A., de Gier, J.W., Ter Beek, J., de Gier, J.-W.W., et al. (2018). Functional and structural characterization of an ECF-type ABC transporter for vitamin B12. Elife *7*, e35828. https://doi.org/10.7554/eLife.35828.
8. Rodionov, D.A., Hebbeln, P., Eudes, A., Ter Beek, J., Rodionova, I.A., Erkens, G.B., Slotboom, D.J., Gelfand, M.S., Osterman, A.L., Hanson, A.D., and Eitinger, T. (2009). A novel class of modular transporters for vitamins in prokaryotes. J. Bacteriol. *191*, 42–51. https://doi.org/10.1128/JB.01208-08.
9. Rempel, S., Gati, C., Nijland, M., Thangaratnarajah, C., Karyolaimos, A., de Gier, J.W., Guskov, A., and Slotboom, D.J. (2020). A mycobacterial ABC transporter mediates the uptake of hydrophilic compounds. Nature *580*, 409–412. https://doi.org/10.1038/s41586-020-2072-8.
10. Gopinath, K., Venclovas, Č., Ioerger, T.R., Sacchettini, J.C., McKinney, J.D., Mizrahi, V., and Warner, D.F. (2013). A vitamin B12 transporter in Mycobacterium tuberculosis. Open Biol. *3*, 120175. https://doi.org/10.1098/rsob.120175.
11. Rempel, S., Colucci, E., de Gier, J.W., Guskov, A., and Slotboom, D.J. (2018). Cysteine-mediated decyanation of vitamin B12 by the predicted membrane transporter BtuM. Nat. Commun. *9*, 3038. https://doi.org/10.1038/s41467-018-05441-9.
12. Finkenwirth, F., Kirsch, F., and Eitinger, T. (2013). Solitary BioY proteins mediate biotin transport into recombinant Escherichia coli. J. Bacteriol. *195*, 4105–4111. https://doi.org/10.1128/JB.00350-13.
13. Kim, J., Gherasim, C., and Banerjee, R. (2008). Decyanation of vitamin B12 by a trafficking chaperone. Proc. Natl. Acad. Sci. USA *105*, 14551–14554. https://doi.org/10.1073/pnas.0805989105.
14. Banerjee, R., and Ragsdale, S.W. (2003). The many faces of vitamin B12: catalysis by cobalamin-dependent enzymes. Annu. Rev. Biochem. *72*, 209–247. https://doi.org/10.1146/ANNUREV.BIOCHEM.72.121801.161828.
15. Brown, K.L., and Wu, G.Z. (1994). Thermodynamics of the Base-On/Base-Off Equilibrium of Alkyl-13-epi- and Alkyl-8-epicobalamins: Understanding the Thermodynamics of Axial Ligand Substitution in Alkylcobalt Corrinoids. Inorg. Chem. *33*, 4122–4127. https://doi.org/10.1021/IC00096A042.
16. Drennan, C.L., Huang, S., Drummond, J.T., Matthews, R.G., Ludwig, M.L., and Lidwig, M.L. (1994). How a protein binds B12: A 3.0 Å x-ray structure of B 12-binding domains of methionine synthase. Science *266*, 1669–1674. https://doi.org/10.1126/science.7992050.
17. Gruber, K., Puffer, B., and Kräutler, B. (2011). Vitamin B12-derivatives—enzyme cofactors and ligands of proteins and nucleic acids. Chem. Soc. Rev. *40*, 4346–4363. https://doi.org/10.1039/c1cs15118e.
18. Li, Z., Mascarenhas, R., Twahir, U.T., Kallon, A., Deb, A., Yaw, M., Penner-Hahn, J., Koutmos, M., Warncke, K., and Banerjee, R. (2020). An Interprotein Co-S Coordination Complex in the B12-Trafficking Pathway.

J. Am. Chem. Soc. *142*, 16334–16345. https://doi.org/10.1021/JACS.0C06590.

19. Mascarenhas, R., Guha, A., Li, Z., Ruetz, M., An, S., Seravalli, J., and Banerjee, R. (2023). Cobalt-Sulfur Coordination Chemistry Drives B12 Loading onto Methionine Synthase. J. Am. Chem. Soc. *145*, 24678–24689. https://doi.org/10.1021/JACS.3C07941.
20. Du, C., Martin, R., Huang, Y., Borwankar, A., Tan, Z., West, J., Singh, N., Borys, M., Ghose, S., Ludwig, R., et al. (2018). Vitamin B12 association with mAbs: Mechanism and potential mitigation strategies. Biotechnol. Bioeng. *115*, 900–909. https://doi.org/10.1002/BIT.26511.
21. Sjuts, H., Dunstan, M.S., Fisher, K., and Leys, D. (2013). Structure of the cobalamin-binding protein of a putative O-demethylase from Desulfitobacterium hafniense DCB-2. Acta Crystallogr. D Biol. Crystallogr. *69*, 1609–1616. https://doi.org/10.1107/S0907444913011323.
22. Mancia, F., Smith, G.A., and Evans, P.R. (1999). Crystal Structure of Substrate Complexes of Methylmalonyl-CoA Mutase. Biochemistry *38*, 7999–8005. https://doi.org/10.1021/BI9903852.
23. Jost, M., Fernández-Zapata, J., Polanco, M.C., Ortiz-Guerrero, J.M., Chen, P.Y.T., Kang, G., Padmanabhan, S., Elías-Arnanz, M., and Drennan, C.L. (2015). Structural basis for gene regulation by a B12-dependent photoreceptor. Nature *526*, 536–541. https://doi.org/10.1038/nature14950.
24. Teale, F.W., and Weber, G. (1957). Ultraviolet fluorescence of the aromatic amino acids. Biochem. J. *65*, 476–482. https://doi.org/10.1042/BJ0650476.
25. Eftink, M.R., and Ghiron, C.A. (1981). Fluorescence quenching studies with proteins. Anal. Biochem. *114*, 199–227. https://doi.org/10.1016/0003-2697(81)90474-7.
26. Singh, J., Petter, R.C., Baillie, T.A., and Whitty, A. (2011). The resurgence of covalent drugs. Nat. Rev. Drug Discov. *10*, 307–317. https://doi.org/10.1038/nrd3410.
27. Rafiee, S., Asadollahi, K., Riazi, G., Ahmadian, S., and Saboury, A.A. (2017). Vitamin B12 Inhibits Tau Fibrillization via Binding to Cysteine Residues of Tau. ACS Chem. Neurosci. *8*, 2676–2682. https://doi.org/10.1021/ACSCHEMNEURO.7B00230.
28. Olson, S.T., Swanson, R., Day, D., Verhamme, I., Kvassman, J., and Shore, J.D. (2001). Resolution of Michaelis complex, acylation, and conformational change steps in the reactions of the serpin, plasminogen activator inhibitor-1, with tissue plasminogen activator and trypsin. Biochemistry *40*, 11742–11756. https://doi.org/10.1021/BI0107290.
29. Weerapana, E., Wang, C., Simon, G.M., Richter, F., Khare, S., Dillon, M.B.D., Bachovchin, D.A., Mowen, K., Baker, D., and Cravatt, B.F. (2010). Quantitative reactivity profiling predicts functional cysteines in proteomes. Nature 468, 790–795. https://doi.org/10.1038/nature09472.
30. Strelow, J.M. (2017). A Perspective on the Kinetics of Covalent and Irreversible Inhibition. SLAS Discov. *22*, 3–20. https://doi.org/10.1177/1087057116671509.
31. Koutmos, M., Gherasim, C., Smith, J.L., and Banerjee, R. (2011). Structural basis of multifunctionality in a vitamin B 12- processing enzyme. J. Biol. Chem. *286*, 29780–29787. https://doi.org/10.1074/jbc.M111.261370.
32. Zhao, Q., Wang, C., Wang, C., Guo, H., Bao, Z., Zhang, M., and Zhang, P. (2015). Structures of FolT in substrate-bound and substrate-released conformations reveal a gating mechanism for ECF transporters. Nat. Commun. *6*, 7661. https://doi.org/10.1038/ncomms8661.
33. Majsnerowska, M., Hänelt, I., Wunnicke, D., Schäfer, L.V., Steinhoff, H.J., and Slotboom, D.J. (2013). Substrate-Induced Conformational Changes in the S-Component ThiT from an Energy Coupling Factor Transporter. Structure *21*, 861–867. https://doi.org/10.1016/J.STR.2013.03.007.
34. Li, Z., Shanmuganathan, A., Ruetz, M., Yamada, K., Lesniak, N.A., Kräutler, B., Brunold, T.C., Koutmos, M., and Banerjee, R. (2017). Coordination chemistry controls the thiol oxidase activity of the B12-trafficking protein CblC. J. Biol. Chem. *292*, 9733–9744. https://doi.org/10.1074/jbc.M117.788554.
35. Youngdahl Turner, P., Rosenberg, L.E., and Allen, R.H. (1978). Binding and uptake of transcobalamin II by human fibroblasts. J. Clin. Invest. *61*, 133–141. https://doi.org/10.1172/JCI108911.
36. McCoy, A.J., Grosse-Kunstleve, R.W., Adams, P.D., Winn, M.D., Storoni, L.C., and Read, R.J. (2007). Phaser crystallographic software. J. Appl. Crystallogr. *40*, 658–674. https://doi.org/10.1107/S0021889807021206.
37. Murshudov, G.N., Skubák, P., Lebedev, A.A., Pannu, N.S., Steiner, R.A., Nicholls, R.A., Winn, M.D., Long, F., and Vagin, A.A. (2011). REFMAC5 for the refinement of macromolecular crystal structures. Acta Crystallogr. D Biol. Crystallogr. *67*, 355–367. https://doi.org/10.1107/S0907444911001314.
38. Emsley, P., Lohkamp, B., Scott, W.G., and Cowtan, K. (2010). Features and development of Coot. Acta Crystallogr. D Biol. Crystallogr. *66*, 486–501. https://doi.org/10.1107/S0907444910007493.

STAR★METHODS

KEY RESOURCES TABLE

REAGENT or RESOURCE	SOURCE	IDENTIFIER
Bacterial and virus strains		
E. coli MC1061	Thermo Fisher	N/A
E. coli ΔFEC	Rempel et al.[11]	N/A
Deposited data		
Crystal structure of BtuM bound to OHCbl	This study	PDB: 8OVV
Crystal structure of BtuM bound to CNCbl	This study	PDB: 8C7P
Crystal structure of Tagged BtuM bound to CNCbl	Rempel et al.[11]	PDB: 6FFV
Oligonucleotides		
nter-8xHisTag-3C-BtuM_NcoI_Forward: CTACTGCCATGGCGCATCATCACCACC ATCACCATCATCTGGAAGTTCTGTTCC AGGGTCCGCTGAATCTGAC	This study	N/A
BtuM_HindIII_Reverse: CAGTAGAAGCTTTCATTAACGTTCACGACGGGTGC	This study	N/A
USER_BtuM-H27A_Forward: AGCGCTCATUGGGCAAGCATTCATAGCCTG	This study	N/A
USER_BtuM-H27A_Reverse: AATGAGCGCUACGGGTCAGCAG	This study	N/A
USER_BtuM-H28A_Forward: AGCCATGCTUGGGCAAGCATTCATAGCCTG	This study	N/A
USER_BtuM-H28A_Reverse: AAGCATGGCUACGGGTCAGCAG	This study	N/A
USER_BtuM-C80S_Forward: ATTTTAGCGTUAGTCCGGCATATTGGCTG	This study	N/A
USER_BtuM-C80S_Reverse: AACGCTAAAAUCGCTAACACCACCCCAG	This study	N/A
Recombinant DNA		
pBAD24	Lifescience market	Model: PVT0709
pBAD24-3C-BtuM	This study	N/A
pBAD24-3C-BtuM-H28A	This study	N/A
pBAD24-3C-BtuM-H27A-H28A	This study	N/A
pBAD24-3C-BtuM-C80S	This study	N/A
Software and algorithms		
Phaser	McCoy et al.[36]	https://www.phaser.cimr.cam.ac.uk/index.php/Phaser_Crystallographic_Software
RefMac5	Murshudov et al.[37]	https://www.ccp4.ac.uk/html/refmac5.html
Coot	Emsley et al.[38]	https://www2.mrc-lmb.cam.ac.uk/personal/pemsley/coot/
Python code	This study	N/A

RESOURCE AVAILABILITY

Lead contact

Further information and requests for resources and reagents should be directed to and will be fulfilled by Dirk J. Slotboom (d.j.slotboom@rug.nl).

Materials availability

All expression plasmids used in this study will be made available on request. This study did not generate new unique reagents.

Data and code availability

- The crystal structures have been deposited at the Protein Data Bank and are publicly available as of the date of publication. Accession numbers are listed in the key resources table.
- All original code is available in Data S1.
- Any additional information required to reanalyse the data reported in this paper is available from the lead contact upon request.

EXPERIMENTAL MODEL AND STUDY PARTICIPANT DETAILS

E. coli MC1061 cells (Thermo Fisher) carrying pBAD24 plasmids containing BtuM variants were cultivated in LB broth containing 100 μg ml^{-1} ampicilin at 37°C.

E. coli ΔFEC cells carrying pBAD24 plasmids containing BtuM variants were cultivated in M9 minimal medium (47.7 mM $Na_2HPO_4 \times 12H_2O$, 17.2 mM KH_2PO_4, 18.7 mM NH_4Cl, 8.6 mM NaCl) supplemented with 0.4 % v/v glycerol, 2 mM $MgSO_4$, 0.1 mM $CaCl_2$, 100 μg ml^{-1} L-arginine and 50 μg ml^{-1} L-methionine; containing 25 μg ml^{-1} kanamycin and 100 μg ml^{-1} ampicillin.

METHOD DETAILS

Molecular methods

A construct of BtuM from *Thiobacillus denitrificans*, including a human Rhinovirus 3C protease cleavage site and an N-terminal histidine-tag, was inserted into a pBAD24 vector (Lifescience Market) using restriction enzymes NcoI and HindIII (New England Biolabs, key resources table).

BtuM mutants C80S, C80A, H28A and the double mutant H27A/H28A were modified from BtuM sequence using USER-cloning site-directed mutagenesis (New England Biolabs, key resources table).

Overexpression and bacterial membranes preparation

Overexpression and preparation of membranes of *E. coli* cells expressing different BtuM variants were conducted as described in (Rempel et al., 2018). *E. coli* strain MC1061 transformed with the appropriate BtuM construct were grown overnight in LB-medium supplemented with 100 μg ml^{-1} ampicillin. Saturated *E. coli* precultures were diluted in fresh LB in a 1:100 ratio and allowed to grow at 37°C to an OD_{600} of 0.6–0.8. Expression was induced by addition of 0.01 % w/v l-arabinose for 3 h. Cells were harvested, washed with 50 mM KPi pH 7.5, 10 % v/v glycerol, flash frozen in liquid nitrogen and stored at -80°C. Cells were disrupted with a high-pressure homogeniser (HPL6, Maximator) at 20 kpsi in the wash buffer supplemented with 200 μM PMSF, 1 mM $MgSO_4$ and DNaseI. Cell debris was removed by centrifugation for 30 min with 25,805 × g and 4°C. The supernatant was centrifuged for 2.5 h at 158,420 × g (average) and 4°C to collect crude membrane vesicles (CMVs). The CMV pellet was homogenized in 50 mM KPi pH 7.5 and used for purification.

Purification of BtuM

BtuM with an N-terminal histidine-tag and a 3C cleavage site was solubilized in solubilization buffer (50 mM HEPES/NaOH pH 8.0, 200 mM NaCl, 0.1 mM CN-Cbl (Merch) or OH-Cbl (Merch), 15 mM imidazole/HCl pH 8.0, 0.5 mM TCEP, 1 % (w/v) *n*-dodecyl-β-D-maltoside (DDM)) (Anatrace) for 45 minutes at 4°C with slow rocking. Insolubilized material was pelleted by centrifugation at 219373 × g at 4°C. The supernatant corresponding to 2 L of cell culture was incubated with 0.5 ml of Superflow Ni^{2+}-NTA Sepharose equilibrated with 20 column volumes (CV) of wash buffer (50 mM HEPES/NaOH pH 8.0, 200 mM NaCl, 50 μM CN-/OH-Cbl, 50 mM imidazole/HCl pH 8.0, 0.5 mM TCEP, 0.35 % (w/v) *n*-nonyl-β-D-glucopyranoside (NG)) (Anatrace). Unbound protein was allowed to flow through and the resin washed with 40 CV wash buffer. The resin, bound to the His-tagged proteins was then resuspended adding 0.2 ml of 3C protease purification buffer containing 1.2 mg of 3C and 50 mM Tris-HCl pH 8.0, 150 mM NaCl, 20 % v/v glycerol, 10 mM EDTA and 1 mM DTT. The final cleavage solution was adjusted to 100 mM imidazole pH 8.0 for an optimal cleavage. The reaction was incubated for 2 hours at 4°C with slow rocking. The cleaved protein was then allowed to flow through using wash buffer. The 3C protease used for this experiment contained an engineered his-tag, remaining attached to the Ni^{2+}-NTA Sepharose resin (Cytiva) after the elution. The tagless BtuM sample was then loaded on a NAP-10 desalting column (Cytiva) for kinetic assays or a Superdex 200 10/300 GL Increase SEC column (Cytiva) for crystallography experiments, using a buffer consisting on 50 mM HEPES/NaOH pH 7.5, 150 mM NaCl, 5 μM CN-/OH-Cbl, 0.5 mM TCEP, 0.35 % (w/v) NG. All buffers for the kinetic assays contained no cobalamin and 0.05 % (w/v) DDM instead of NG.

Crystallography experiments

Purified *holo*-BtuM, bound during purification to either CNCbl or OHCbl was concentrated to ~8 mg ml^{-1} with a 50 kDa cut-off Vivaspin concentrator (Sartorius) at 4°C. Initial crystallization screening was performed using a Mosquito robot (TTP Labtech). A hit was found in the condition B11 (0.2 M KCl, 0.1 M sodium citrate pH 5.5, 37 % v/v pentaerythritol propoxylate) of the MemGold screen (Molecular Dimensions) at 4°C. Larger bar-shaped crystals of a characteristic pink colour were obtained in a crystallization condition containing a similar composition that was prepared using the Dragonfly plate optimiser (SPT Labtech) in sitting drop vapor diffusion

MRC-2 welled plates with 50 μl of reservoir and 2:1 protein-to-reservoir ratio (300 μl final drop volume). Both OH- and CNCbl-bound BtuM yielded crystals diffracting to 1.86 and 2.53 Å resolution, respectively.

Crystallisation, phasing and structure determination

Diffraction data from the native crystals were collected at the Diamond Light Source (DLS) at I24 beamline (λ = 1.000 Å, T = 100 K). Data were processed with XDS (version 20220820). Both datasets were anisotropic, and anisotropy correction was implemented using StarAniso (version v3.350) on the dataset of BtuM-OHCbl. The phases were calculated using PHASER (version 2.7.0) using the previous BtuM structure (PDB: 6FFV) as a model for molecular replacement. The obtained solution was refined in iterative cycles using RefMac5 and manual adjustments were done in COOT (version 0.9.4.1). During refinement, a resolution cut-off of 2.26 Å for BtuM-OHCbl and 3.0 Å for BtuM-CNCbl was applied to address the low completeness at high resolution. In addition, BtuM-OHCbl was corrected for twinning during refinement. All structural figures were prepared with an open-source version of PyMOL (https://sourceforge.net/projects/pymol/).

Growth assay

The growth assay was conducted as described in Rempel et al., 2018. 5 ml M9 minimal medium (47.7 mM $Na_2HPO_4 \times 12H_2O$, 17.2 mM KH_2PO_4, 18.7 mM NH_4Cl, 8.6 mM NaCl) was supplemented with 0.4 % v/v glycerol, 2 mM $MgSO_4$, 0.1 mM $CaCl_2$, 100 μg ml^{-1} L-arginine, 25 μg ml^{-1} kanamycin, 100 μg ml^{-1} ampicillin and 50 μg ml^{-1} L-methionine (Sigma-Aldrich); and inoculated with *E. coli* ΔFEC strains carrying the various expression vectors and grown overnight at 37°C. The pre-culture was grown ~24 h at 37°C, shaking in tubes with gas-permeable lids (Cellstar), and then used to inoculate the assay medium in a 1:500 ratio. The assay medium was supplemented with 0.00001 % w/v L-arabinose (Sigma-Aldrich) and 0.1 nM cyanocobalamin (Acros Organics) instead of 50 μg ml^{-1} L-methionine. Overall, 200 μl medium was added per well on a sterile 96 well plate (Cellstar). Plates were sealed with a sterile and gas-permeable foil (BreatheEasy, Diversified Biotech). The cultures were grown for 1000 min in a BioTek Power Wave 340 plate reader at 37°C, shaking. The OD_{600} was measured every 5 min at 600 nm. All experiments were conducted as technical triplicates from biological duplicates.

Absorbance kinetic assay

A quartz 96-well plate was filled with the different purified BtuM constructs, every well was loaded with the indicated concentration of CNCbl, OHCbl or Cbi and the absorbance was scanned between 250 and 600 nm for up to 12 hours. The substrate saturation was calculated making the difference between the absorbance peak and a linear regression between 325 nm and 400 nm (bottom of absorbance). Absorbance values over time were normalized against the value at time 0, which was assigned a value of 0.0 (representing a 0% fraction of protein-bound substrate). At saturating conditions (protein:substrate molar ratio of 3:1), the absorbance peak is indistinguishable. Therefore, in saturating conditions, the absorbance peak is 0, and the substrate fraction of saturated substrate is 1.0. Any intermediate value between 0.0 and 1.0 represents the fraction of substrate bound to BtuM. Two technical replicates of Cbi absorbance kinetic measurements were used to feed the 2-step irreversible binding model. Results were processed using R studio.

Tryptophan fluorescence kinetic assay

Emission at 330 nm was detected upon excitation at 280 nm using a quartz cuvette filled with 2 ml of untagged BtuM purified in DDM solution at 25°C and 750 rpm magnet stirring in a JASCO F8300 device. Fluorescence was measured every 1 minute after addition of Cbi and every 10 minutes for CNCbl and OHCbl. The results are referenced against a control with no added substrate. The resulting decay over time was normalized against the initial value at 0 minutes, when the saturation is 0.0. The fluorescence decay in saturating conditions (10:1 substrate:BtuM ratio) was assigned a saturation value of 1.0. Any intermediate value between 0.0 and 1.0 represents the fraction of BtuM bound to the substrate. The irreversible binding model was fitted using 4 sets of 4 different ligand:protein ratios at different initial protein concentrations (for an overview of the model, see Suppl. Info. 1).

QUANTIFICATION AND STATISTICAL ANALYSIS

For this work, averages and standard deviations were calculated. No methods to determine whether the data met assumptions of the statistical approach were used. The description of statistical measures can be found in the figure legends of applicable experiments. The description of the number of replicates *n* can be found in the method details section.

X-ray data collection and refinement statistics are reported in Table 1.